Journal of Systems Engineering and Electronics
Vol. 37, No. 3, June 2026, pp.861 – 866

Dual-frequency aperiodic planar scanning array with diversified radiation elements

JIANG Hailing* and DU Ke

Hebei Key Laboratory of Electromagnetic Spectrum Cognition and Control, The 54th Research Institute of China Electronics Technology Group Corporation, Shijiazhuang 050081, China

Abstract: A dual-frequency aperiodic planar scanning array with diversified radiation elements is proposed. The proposed element consists of an elliptic patch and two parasitic rectangular patches, which can work both at 5.28–5.33 GHz with difference radiation beam and 5.78–5.83 GHz with sum radiation beam. A four equivalent magnetic currents model has been established to explain the radiation principle of the proposed element. Compared to the beamwidth of the sum beam, the 3 dB beamwidth of the difference beam is broadened about 30% and the radiation gain of the sum beam is obviously improved about 48%. A 64-element aperiodic array with diversified radiation elements is constructed. The array can scan at a wide angle of ±70° with no grating lobes at difference radiation mode and can scan in the range of ±60° with high gain at sum radiation mode.

Keywords: aperiodic array, diversified radiation, high gain, wide beamwidth, magnetic current, wide-angle scan.

DOI: 10.23919/JSEE.2026.000109

1. Introduction

Nowadays, wireless communication systems tend to move towards high capacity, wide coverage, high connectivity and low energy consumption [1]. To meet these requirements, wireless communication system frontend antennas need to be functionally diversified. For example, some 5G application scenarios require a single antenna to operate on more frequency bands [2–6], more polarization [7], more pattern shapes [8–9], at the same aperture, which increases the complexity of different feed ports and networks. Therefore, an antenna with multi-bands and a shared feed port can reduce the cost of the communication system and be easier to be integrated into radio frequency (RF) circuits. Compared with broadband antennas [10–11], multi-bands antennas can achieve different polarizations [12–14], different radiation patterns [15], or different stopbands [16] in different operating bands. References [17] and [18] give some typical methods for dual-band antenna design, but the design of multi-band antennas still faces technical difficulties such as multi-feed, complex structure, high profile and so on. On the other hand, antennas with wide beamwidth have great potential to broaden the scanning angle of phased arrays [19–25], and antennas with high radiation gain can increase the channel capacity of wireless communication systems [26–30].

Therefore, it is necessary to design a dual-band diversified antenna with a wide radiation beamwidth in one frequency band and high radiation gain in the other frequency band. The diversified radiation patterns can make it have a wider range of applications.

This paper provides a dual-band element with diversified radiation patterns for diverse wireless communication systems. The radiation patterns of the two operating frequency bands have different salient features. In the low frequency band, the radiation beamwidth can reach more than 98°, and in the high frequency band, the radiation gain can reach to 7.19 dB. In addition, a 64-element aperiodic array with above proposed elements is designed. In the low frequency band, the array scans at a wide angle of ±70° with no grating lobes at difference radiation mode and in the high frequency band, it can scan in the range of ±60° with high gain at sum radiation mode.

2. Element design and analysis

2.1 Element structure

The proposed element printed on a dielectric substrate with a relative dielectric constant of 6.6 and a thickness of h, is shown in Fig. 1. According to the requirements of diversified radiation patterns, the models of central radiation patch and lateral parasitic patch are established.

Manuscript received August 07, 2024.
*Corresponding author.

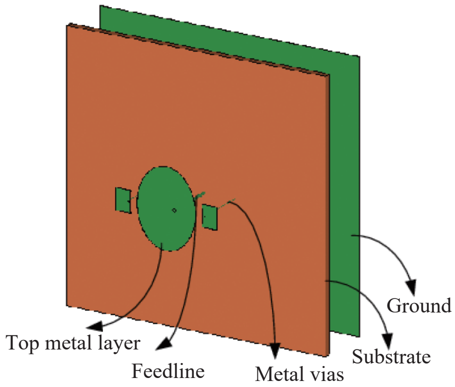

(a) Three-dimensional view

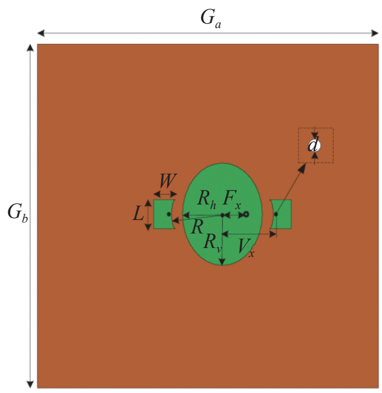

(b) Top view

Fig. 1 Structure of the antenna

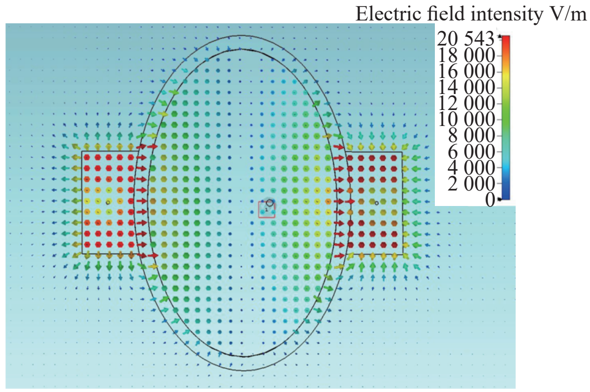

(a) Electric field intensity@5.3 GHz

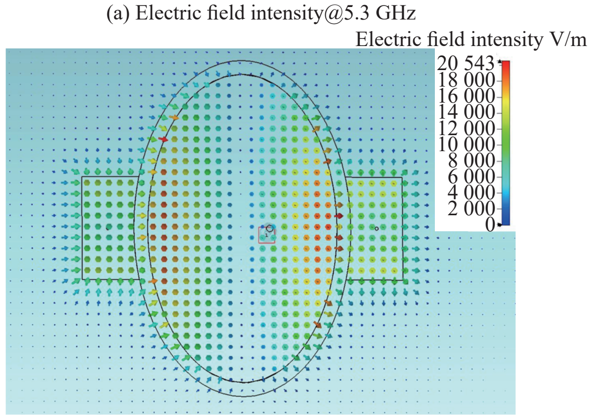

(b) Electric field intensity@5.8 GHz

Fig. 2 Electric field distribution of the antenna

An elliptic patch with a major radius of R_v and a minor radius of R_h is in the center. Two rectangular parasitic patches are on both sides with a length of L and a width of W. Two metallized vias with a diameter of d are placed separately at specific positions in the two rectangular patches to connect the patches and the ground. Two gaps are formed between the elliptic patch and the rectangular patches on both sides. To obtain a better matching effect, we feed at a position F_x deviating from the center of the elliptic patch.

The initial parameter values are set according to the operating wavelength, and then the parameters are adjusted through optimization. These specific geometrical parameters are $W = 3$ mm, $R = 6.3$ mm, $L = 6$ mm, $R_h = 5.5$ mm, $R_v = 9$ mm, $G_a = 50$ mm, $d = 0.2$ mm, $G_b = 50$ mm, $F_x = 1.6$ mm, V_x=7.8 mm, $h = 0.8$ mm.

2.2 Radiation principle

Fig. 2(a) shows the surface electric field distribution of the proposed antenna at 5.3 GHz. The electric fields are mainly concentrated on the gaps between the elliptic patch and the rectangular patches as well as the two outer edges of the rectangular patches in x direction.

Similarly, Fig. 2(b) shows the surface electric field distribution of the proposed antenna operating at 5.8 GHz. Different from Fig. 2(a), the directions of the electric fields in the outer sides of the rectangular patches are reversed.

The radiation principle of the proposed antenna can be explained by a four equivalent magnetic currents model (FEMCM) array. From Fig. 2, the four equivalent magnetic currents are mainly generated by the position of the gaps and outer edges where the electric field is concentrated. The individual magnetic current can be controlled by changing the size of the elliptic patch, the size of the rectangular patch, and the gap between the elliptic patch and the rectangular patch.

Fig. 3(a) shows the FEMCM when the antenna operating at 5.3 GHz. It should be noticed that the directions of the equivalent magnetic currents in the gaps between the elliptic patch and the parasitic rectangular patches are opposite to that of the two outer of the parasitic rectangular patches. In this case, it is named difference beam and its radiation pattern can be calculated by expression [31] below:

$$F_1 = -B_1\cos(kh\cos\theta) + A_1\cos(kh\cos\theta)\mathrm{e}^{\mathrm{j}\frac{2\pi}{\lambda}d_1\sin\theta\cos\varphi} + A_1\cos(kh\cos\theta)\mathrm{e}^{\mathrm{j}\frac{2\pi}{\lambda}(d_1+d_2)\sin\theta\cos\varphi} - B_1\cos(kh\cos\theta)\mathrm{e}^{\mathrm{j}\frac{2\pi}{\lambda}(d_1+d_2+d_3)\sin\theta\cos\varphi}, \quad (1)$$

$$F_2 = B_2\cos(kh\cos\theta) + A_2\cos(kh\cos\theta)\mathrm{e}^{\mathrm{j}\frac{2\pi}{\lambda}d_1\sin\theta\cos\varphi} + A_2\cos(kh\cos\theta)\mathrm{e}^{\mathrm{j}\frac{2\pi}{\lambda}(d_1+d_2)\sin\theta\cos\varphi} + B_2\cos(kh\cos\theta)\mathrm{e}^{\mathrm{j}\frac{2\pi}{\lambda}(d_1+d_2+d_3)\sin\theta\cos\varphi} \quad (2)$$

where F_1 and F_2 are radiation patterns. A_1 and B_1 respectively represent the amplitudes of the equivalent magnetic currents I_{c1} and I_{r1} shown in Fig. 3(a). By comparing the color distribution of the electric field intensity in Fig. 2(a), the amplitude ratio of the magnetic current at the corresponding position can be obtained. As can be seen from Fig. 2(a), A_1 is about twice as large as B_1. k is the wave number in a dielectric substrate. h is the distance between the magnetic currents and the ground, which is the thickness of the dielectric substrate. As shown in Fig. 3(a), d_1, d_2 and d_3 represent the distances between the magnetic currents. Fig. 3(c) shows the calculated radiation pattern of the proposed antenna working at 5.3 GHz. The calculated beamwidth of the proposed antenna is about 116°.

Similarly, Fig. 3(b) shows the FEMCM when the proposed antenna operating at 5.8 GHz. Since the directions of the equivalent magnetic currents in the gaps between the elliptic patch and the parasitic rectangular patches are the same as ones from the two outer sides of the rectangular patches, it is named sum beam. Its radiation pattern can be calculated by expression (2), where A_2 and B_2 represent the amplitudes of the equivalent magnetic currents I_{c2} and I_{r2} shown in Fig. 3(b), respectively. According to the color distribution of the electric field intensity in Fig. 2(b), it is obtained that A_2 is much larger than B_2. Fig. 3(d) shows the calculated radiation pattern of the proposed antenna which has high radiation gain with narrow beamwidth. It should be illustrated that the main polarizations of the proposed antenna working in both operating bands are horizontal-polarized.

From the above analysis, it can be seen that the proposed antenna has diversified radiation patterns, which can achieve wide beam radiation in the low frequency band and high gain radiation in the high frequency band. Fig. 3(c) and Fig. 3(d) also show the simulated radiation patterns of the proposed element, from which, the calculated results are highly consistent with the simulation in the range of 3 dB beamwidth. In Fig. 3(d) there are some deviations in the end fire direction, because the ground plane is infinite in theory, and it is finite in simulation.

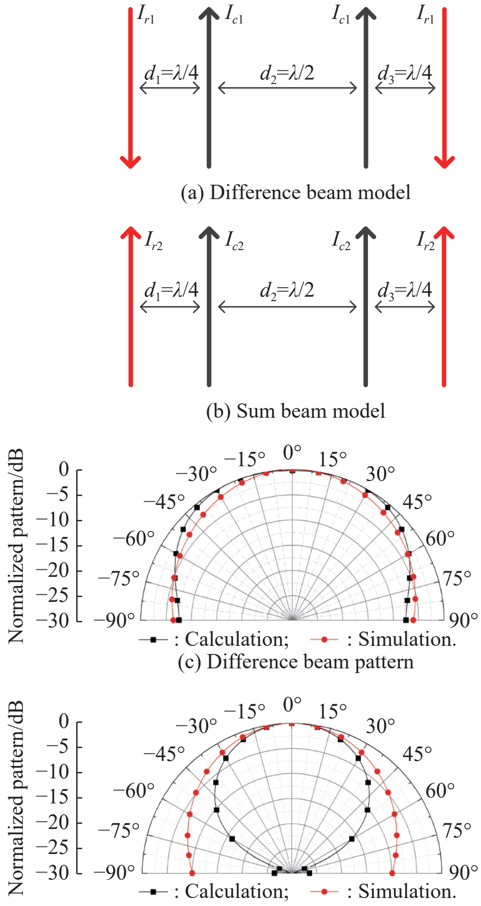

(a) Difference beam model
(b) Sum beam model
(c) Difference beam pattern
(d) Sum beam pattern

Fig. 3 Four magnetic currents models and radiation patterns

2.3 Working performance

Fig. 4(a) shows the measured photograph of the proposed antenna. The measured reflection coefficient of the proposed element is shown in Fig. 4(b). The proposed antenna has two operating frequency bands of 5.28−5.38 GHz and 5.78−5.83 GHz with the reflection coefficient $|S_{11}| \leqslant -10$ dB.

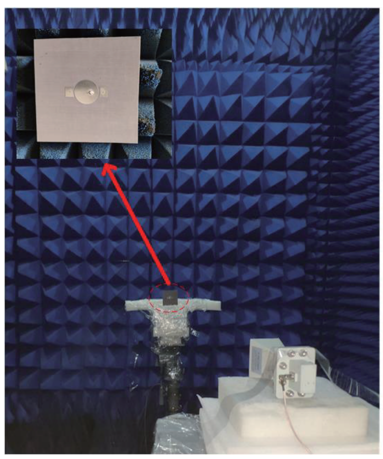

(a) Measured photograph

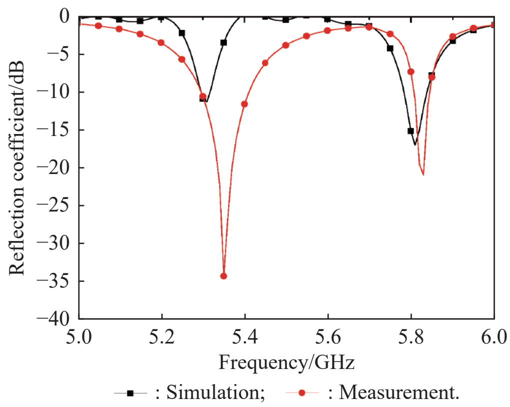

(b) Measured reflection coefficient

Fig. 4 Measured photograph and results

As can be seen from Fig. 4, there are some differences between the measurement results of reflection coefficient and the simulation results, which are mainly due to the dielectric constant error of the substrate, manufacturing errors and measurement errors. Generally speaking, the measured results of high band are in good agreement with the simulation results, while the measured results of low band are slightly offset.

Fig. 5 shows the measured radiation patterns of the proposed element in the xoz plane and a comparison of the radiation patterns between sum beam and difference beam.

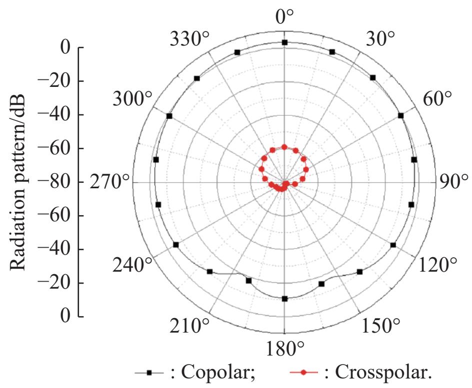

(a) Radiation pattern@5.3 GHz

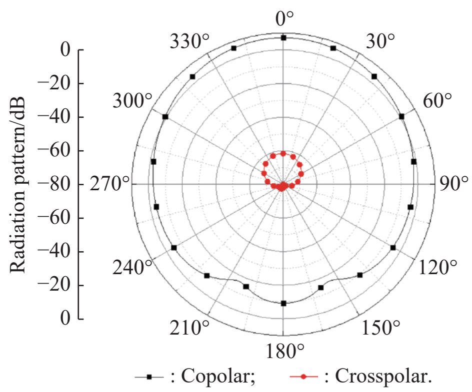

(b) Radiation pattern@5.8 GHz

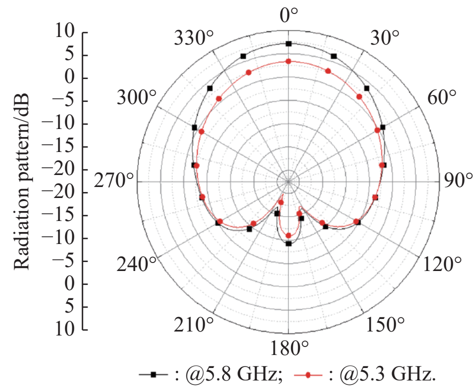

(c) Comparison results

Fig. 5 Radiation patterns and comparison results

From Fig. 5, in the lower band, the proposed element has a 3 dB beamwidth of 98° and a radiation gain of 3.3 dB. In the higher band, the proposed element has a high radiation gain of 7.19 dB and 3 dB beamwidth of 75°. The proposed element can achieve diversified radiation patterns. Firstly, when the proposed element works in the lower frequency band, the 3 dB beamwidth is expanded about 30%. Secondly, when the proposed element works in the higher frequency band, the gain of the proposed antenna increases about 48%. As a result, the proposed element has dual-band and multifunctional radiation characteristics.

3. Array design and analysis

The aperiodic array structure with horizontal spacing larger than 0.5λ is shown in blue circles in Fig. 6(a). The periodic array is uniformly arranged at 0.5λ spacing in y-axis and 0.9λ spacing in x-axis as shown in red squares, where λ is the wavelength of 5.8 GHz. Then, the positions of the initial columns and the final columns are changed inward to maintain the total array aperture. After that, the internal elements can change their positions in the range of $[-0.2\lambda, 0.2\lambda]$. Finally, a genetic algorithm is used to optimize these positions, in order to achieve low grate lobe levels of the aperiodic array in the scanning range.

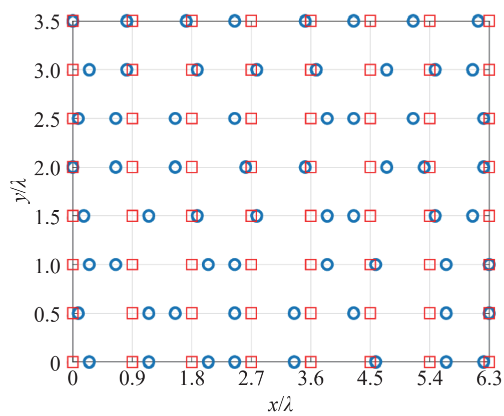

(a) Position of each element

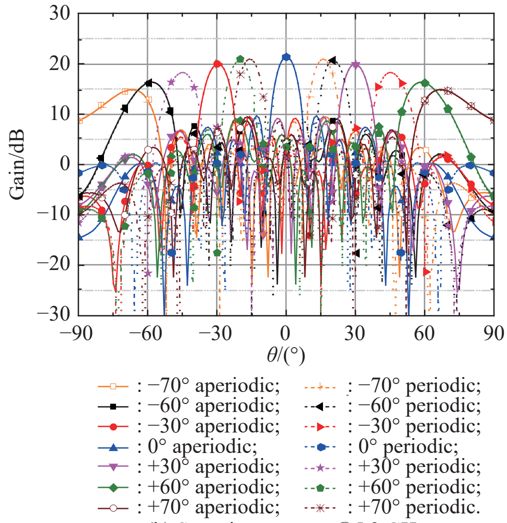

(b) Scanning patterns @5.3 GHz

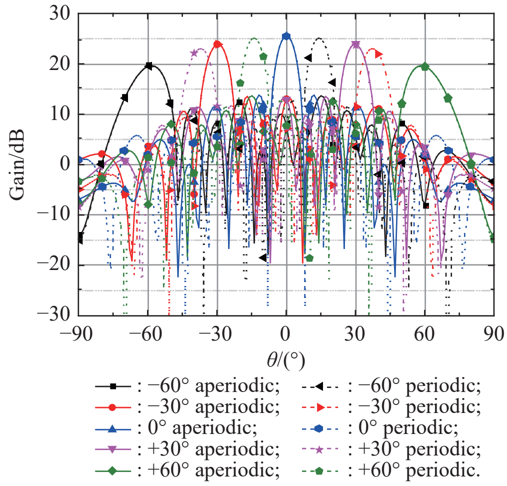

(c) Scanning patterns @5.8 GHz

Fig. 6 Aperiodic array and periodic array

The optimized positions of the aperiodic array are shown in the blue circles in Fig. 6(a). The scanning patterns in the *xoz* plane are shown in Fig. 6(b) and Fig. 6(c).

The results show that the proposed aperiodic array can scan its main lobes from −70° to +70° with the grate lobes below −11.5 dB at difference radiation mode in Fig. 6(b). The main lobe gain is 21.3 dB at broadside, and the main lobe gain decreases 6.5 dB at $\theta = -70°$. In Fig. 6(c), the proposed array can scan its main lobes from −60° to +60° with the grate lobes below −11.7 dB at sum radiation mode. The main lobe gain is 25.5 dB at broadside, which is almost the full aperture gain $4\pi A/\lambda^2$, where A is the array aperture. It should be pointed that the scanning gain of sum mode is significantly higher than that of difference mode, because the element of sum mode has higher radiation gain. The difference mode scan angle is larger, because the beam width of the difference mode element is wider.

4. Conclusions

In this paper, a dual-band microstrip patch element and an aperiodic planar array with wide-angle scanning and high gain are proposed. Based on the principle of electromagnetic superposition, a FEMCM is presented to analyze the element. The proposed multifunctional element works in different frequency bands with different radiation patterns, which can be applied to multifunctional communication systems. The proposed aperiodic planar array also provides an option possibility for macro base stations.

References

[1] HONG W, JIANG Z H, YU C, et al. Multibeam antenna technologies for 5G wireless communications. IEEE Trans. on Antennas and Propagation, 2017, 65(12): 6231–6249.

[2] SYRYTSIN I, ZHANG S, PEDERSEN G F, et al. User effects on the circular polarization of 5G mobile terminal antennas. IEEE Trans. on Antennas and Propagation, 2018, 66(9): 4906–4911.

[3] QIAN J F, CHEN F C, CHU Q X, et al. A novel electric and magnetic gap-coupled broadband patch antenna with improved selectivity and its application in MIMO system. IEEE Trans. on Antennas and Propagation, 2018, 66(10): 5625–5629.

[4] CHEN D X, YANG W C, CHE W Q, et al. Broadband stable-gain multiresonance antenna using nonperiodic square-ring metasurface. IEEE Antennas and Wireless Propagation Letters, 2019, 18(8): 1537–1541.

[5] HUANG D W, DU Z W, WANG Y. A quad-antenna system for 4G/5G/GPS metal frame mobile phones. IEEE Antennas and Wireless Propagation Letters, 2019, 18(8): 1586–1590.

[6] LI Y X, CHU Q X. Dual-band base station antenna array using the low-band antenna as parasitic decoupler. IEEE Antennas and Wireless Propagation Letters, 2022, 21(7): 1308–1312.

[7] CHEN M L, HU H Q, LEI S W, et al. A 3-D pattern-reconfigurable antenna array with multipolarization. IEEE Antennas and Wireless Propagation Letters, 2023, 22(9): 2105–2109.

[8] FENG B T, TU Y T, CHUNG K L, et al. A beamwidth reconfigurable antenna array with triple dual-polarized magneto-electric dipole elements. IEEE Access, 2018, 6(7): 36083–36091.

[9] WANG Z, ZHAO S N, DONG Y D. Pattern reconfigurable, low-profile, vertically polarized, ZOR-metasurface antenna for 5G application. IEEE Trans. on Antennas and Propagation, 2022, 70(8): 6581–6591.

[10] JI Z Q, SUN G H, WONG H. A wideband circularly polarized complementary antenna for millimeter-wave applications. IEEE Trans. on Antennas and Propagation, 2022, 70(4): 2392–2400.

[11] ZHU Y Y, WANG J P, CHEN J X, et al. A compact wideband dual-polarized antenna using monolithic dielectric for 5G base station application. IEEE Antennas and Wireless Propagation Letters, 2022, 21(9): 1717–1721.

[12] PENG L, WEN B J, LI X F, et al. CPW fed UWB antenna by EBGs with wide rectangular notched-band. IEEE Access, 2016, 4: 9545–9552.

[13] LI Y Z, YANG W C, XUE Q, et al. A miniaturized dual-polarized tri-band antenna based on multimode and stacked scheme for multiband aperture-shared base-station applications. IEEE Trans. on Antennas and Propagation, 2024, 72(5): 4647–4652.

[14] LI Y J, YE L H, LI J F, et al. Triband dual-polarized dipole antenna with controllable bandwidths for 5G/LTE applications. IEEE Antennas and Wireless Propagation Letters, 2024, 23(2): 563–567.

[15] LI H, KANG L, WEI F, et al. A low-profile dual-polarized microstrip antenna array for dual-mode OAM applications. IEEE Antennas and Wireless Propagation Letters, 2017, 16: 3022–3025.

[16] ZHANG K, JIANG Z H, ZHOU W L, et al. A compact, band-notched ultra-wideband fully-recessed antenna with pattern diversity for V2X communications. IEEE Open Journal of Antennas and Propagation, 2022, 3: 1302–1312.

[17] WU Z, LI L, CHEN X, et al. Dual-band antenna integrating with rectangular mushroom-like superstrate for WLAN applications. IEEE Antennas and Wireless Propagation Letters, 2016, 15: 1269–1272.

[18] KUMAR P, DWARI S, SAINI R K, et al. Dual-band dual-sense polarization reconfigurable circularly polarized antenna. IEEE Antennas and Wireless Propagation Letters, 2019, 18(1): 64–68.

[19] SUN B F, DING X, CHENG Y F, et al. Substrate integrated waveguide-slot wide-angle scanning aperiodic phased array with low side-lobe levels. Microwave and Optical Technology Letters, 2020, 62(1): 210–216.

[20] DING X, CHENG Y F, SHAO W, et al. A wide-angle scanning planar phased array with pattern reconfigurable magnetic current element. IEEE Trans. on Antennas and Propagation, 2017, 65(3): 1434–1439.

[21] DING X, WANG B Z, HE G Q. Research on a millimeter-wave phased array with wide-angle scanning performance. IEEE Trans. on Antennas and Propagation, 2013, 61(10): 5319–5324.

[22] SUN B F, DING X, CHENG Y F, et al. 2-D wide-angle scanning phased array with hybrid patch mode technique. IEEE Antennas and Wireless Propagation Letters, 2020, 19(4): 700–704.

[23] LIU S H, LIU H M, MA T, et al. Circularly polarized spherical-conformal dielectric resonator antenna with wideband and wide beamwidth. Proc. of the Photonics & Electromagnetics Research Symposium, 2024. DOI: 10.1109/PIERS62282.2024.10618352.

[24] LUO H Y, JIN F L, DING X, et al. Design of wide-scanning array with reactive splitter network and metasurface. Journal of Systems Engineering and Electronics, 2025, 36(2): 323–332.

[25] DING X, RAO L W, FENG B T, et al. A dual-polarized wide-beam antenna array with stable high gain for WiFi-6E (U-NII 6-GHz) communications. IEEE Access, 2024, 12(7): 114573–114583.

[26] JU J, KIM D, LEE W J, et al. Wideband high-gain antenna using metamaterial superstrate with the zero refractive index. Microwave and Optical Technology Letters, 2009, 51(8): 1973–1976.

[27] NAHAS M. A high-gain dual-band LI-slotted microstrip patch antenna for 5G cellular mobile phones. Engineering, Technology & Applied Science Research, 2024, 14(3): 14504-14508.

[28] ZHANG J P, MAO J J. A high-gain Ka-band microstrip patch antenna with simple slot structure. Proc. of the International Conference on Microwave and Millimeter Wave Technology , 2020. DOI: 10.1109/ICMMT49418.2020.9386991.

[29] BARTHWAL A, ARA S. Dual band, high gain simple structure in microstrip patch antenna for X-band application. International Journal for Research Trends and Innovation, 2023, 8(3): 299–303.

[30] FENG L Y, ZHANG C Q. Compact magneto-electric dipole director loaded high-gain dual-polarized magneto-electric dipole antenna. IEEE Antennas and Wireless Propagation Letters, 2024, 23(7): 2130–2134.

[31] MAILLOUX R. Phased array antenna handbook. 3rd Edition. Boston: Artech House, 2017.